European Journal of Medicinal Chemistry 183 (2019) 111720

Contents lists available at ScienceDirect

European Journal of Medicinal Chemistry

journal homepage: http://www.elsevier.com/locate/ejmech

Research paper

Dual-targeting liposomes with active recognition of $GLUT_5$ and $\alpha_v\beta_3$ for triple-negative breast cancer

Yanchi Pu [a], Hao Zhang [a], Yao Peng [a], Qiuyi Fu [a], Qiming Yue [a], Yi Zhao [a, b], Li Guo [a, **], Yong Wu [a, *]

[a] Key Laboratory of Drug-Targeting and Drug Delivery System of the Education Ministry, Sichuan Engineering Laboratory for Plant-Sourced Drug, Sichuan Research Center for Drug Precision Industrial Technology, West China School of Pharmacy, Sichuan University, Chengdu, 610041, PR China
[b] Department of Translational Medicine Center, The First Affiliated Hospital of Zhengzhou University, Zhengzhou, 450052, PR China

ARTICLE INFO

Article history:
Received 18 June 2019
Received in revised form
24 August 2019
Accepted 18 September 2019
Available online 18 September 2019

Keywords:
Liposome
Dual-targeting
TNBC
Fructose
RGD peptide

ABSTRACT

At present, chemo- and radiotherapies remain to be the mainstream methods for treating triple-negative breast cancer (TNBC), which is known for poor prognosis and high rate of mortality. Two types of novel dual-targeting TNBC liposomes (Fru-RGD-Lip and Fru+RGD-Lip) that actively recognize both fructose transporter $GLUT_5$ and integrin $\alpha_v\beta_3$ were designed and prepared in this work. Firstly, a Y-shaped Fru-RGD-chol ligand, where a fructose and peptide Arg-Gly-Asp (RGD) were covalently attached to cholesterol, was designed and synthesized. Then, the Fru-RGD-Lip was constructed by inserting Fru-RGD-chol into liposomes, while Fru+RGD-Lip was obtained by inserting both Fru-chol and RGD-chol (with the molar ratio of 1:1) into liposomes. The particle size, zeta potential, encapsulation efficiency and serum stability of the paclitaxel-loaded liposomes were characterized. The results indicated that the paclitaxel-loaded Fru-RGD-Lip had the strongest growth inhibition against $GLUT_5$ and $\alpha_v\beta_3$ overexpressed MDA-MB-231 and 4T1 cells. The cellular uptake of Fru-RGD-Lip on MDA-MB-231 cells and 4T1 cells was 3.19- and 3.23-fold more than that of the uncoated liposomes (Lip). The uptake of Fru+RGD-Lip was slightly lower, giving a 2.81- and 2.90-fold increase than that of Lip in two cell lines, respectively. The mechanism study demonstrated that the cellular uptake of both dual-targeting liposomes was likely to be recognized and mediated by $GLUT_5$ and $\alpha_v\beta_3$ firstly, then endocytosed through comprehensive pathways in an energy-dependent manner. Moreover, Fru-RGD-Lip displayed the maximum accumulation, which was 2.62-fold higher than that of Lip for instance, at the tumor sites compared to other liposomes using *in vivo* imaging. Collectively, the liposomes co-modified by fructose and RGD have enormous potential in the development of targeted TNBC treatment, especially the covalently modified Fru-RGD-Lip, making it a promising multifunctional liposome.

1. Introduction

Globally, breast cancer has the highest incidence among women. As a malignant tumor, it seriously affects women's health [1]. Triple-negative breast cancer (TNBC), with deficiencies of estrogen receptor (ER), progesterone receptor (PR), and human epidermal growth factor receptor 2 (Her-2), is one of the most invasive subtypes of breast cancer, accounting for approximately 20% of all breast cancer [2,3]. The drugs normally used to treat breast cancer are ineffective against TNBC due to the loss of therapeutic targets. At present, the main treatments of TNBC are still surgery, chemotherapy and radiotherapy, with poor prognosis and quite high mortality rate [4]. Therefore, the dilemma faced by TNBC is urgently to be alleviated.

Commonly used chemotherapeutic drugs, such as paclitaxel (PTX) and doxorubicin (DOX), are highly toxic to normal cells. Therefore, one approach to increase their efficacy is to enhance the selectivity of such drugs, so that higher dose of drugs could be applied [5]. Current research are mainly focused on designing novel targeting drug delivery system (TDDS) [6]. What attracts much attention is to search ligands that can selectively bind with specific receptors and/or transporters, such as glucose transporters, integrin receptors, folate receptors, and ferritin receptors and etc [7],

* Corresponding author.
** Corresponding author.
E-mail addresses: guoli@scu.edu.cn (L. Guo), wyong@scu.edu.cn (Y. Wu).

https://doi.org/10.1016/j.ejmech.2019.111720
0223-5234/

overexpressed at the target sites (especially cancer cells).

The metabolic behavior of tumor is different from normal cells, characterized by the sharp increase of glucose uptake and glycolysis even in oxygen sufficient conditions, which was known as the Warburg effect [8]. Hence, the rapid proliferation and Warburg effect make a large amount of glucose consumption, causing a low-glucose microenvironment in cancer cells [9]. D-fructose, the second most abundant monosaccharide in nature, is largely used by cancer cells to alleviate the deficiency of energy. Therefore, the cellular uptake of fructose in breast cancer is much more than that of the normal breast cells, and even for other tumor cells are 8–10 times higher. Yet the uptake of glucose in breast cancer cells is only slightly changed comparing to normal breast cells [10–12]. Among the 14 subtypes of hexose transporters (GLUTs), only $GLUT_2$ and $GLUT_5$ were able to transport fructose [13]. The substrate of $GLUT_5$ is almost only fructose, and about 90% of fructose is transported by $GLUT_5$ [14,15]. Therefore, $GLUT_5$ is a specific transporter for fructose. $GLUT_5$ has been reported to be overexpressed in breast cancer cells and tumor tissues, but not in their normal counterpart [16–18]. Thus, the substrate specificity of $GLUT_5$ and its relatively concentrated expression tissue site give it the advantage to be an efficient target for the diagnosis and treatment of TNBC [19–21].

In addition to the GLUTs, integrin receptors, which are considered as a biomarker of tumors, are also overexpressed in many tumor cells and neovascular endothelial cells. Integrins belong to the transmembrane glycoprotein family, and mediate cell-cell and cell-matrix interactions [22], which is related to the adhesion and migration of tumor cells and the formation of tumor blood vessels [23,24]. Among the 26 subtypes, $\alpha_v\beta_3$ is the most concerned [25]. Various subtypes of integrin receptors can recognize the same peptide Arg-Gly-Asp (RGD). Therefore, RGD is broadly used as a specific ligand for integrins. It has been widely reported that $\alpha_v\beta_3$ is overexpressed on the surface of a variety of tumor cells, including triple-negative breast cancer cells [26]. Therefore, $\alpha_v\beta_3$ may act as a promising target of TNBC.

Fructose [21] and RGD as well as their derivatives [27] have been reported to be individually conjugated with nanocarriers for targeting TNBC. However, the targeting ability mediated by a single receptor or transporter can hardly achieve the expectation. So, to utilize more than one receptor that is specifically overexpressed on the tumor cells may further enhance the targeting ability. The dual-targeting strategy has been confirmed by many reports, such as glucose and RGD co-modified liposomes [28], p-aminophenyl-α-D-mannopyranoside (MAN) and transferrin (TF) co-modified daunorubicin liposomes [29], and etc. In this work, by targeting both $GLUT_5$ and $\alpha_v\beta_3$ that are overexpressed on TNBC cells, we report two types of novel liposomes co-modified with fructose and RGD to improve the targeting ability. One is by physical mixing of two ligands (with the molar ratio of 1:1) with the liposome (Fru+RGD-Lip). The other is to covalently link two ligands first to form a Y-shaped ligand with both fructose and RGD, then mixed with the liposomes (Fru-RGD-Lip). The characteristics of liposomes and their targeting ability to TNBC were evaluated *in vitro* and *in vivo*.

2. Results and discussion

2.1. Synthesis of liposomes ligands

According to the structure-activity relationship of the specific affinity between fructose and $GLUT_5$, and the phosphorylation of fructose when metabolized in TNBC cells, the fructose can only be modified on C1–OH [30–32]. Moreover, for the RGD tripeptide, it has little impact on affinity when modifying the primary amino group [33], while the other groups are essential for binding to $\alpha_v\beta_3$. Therefore, the Y-shaped ligand (Fru-RGD-chol) for dual-targeting TNBC was designed and synthesized with fructose and RGD peptide as targeting molecules, lysine as a linker and cholesterol as a lipid material, in which C1–OH of fructose and primary amino group of RGD were the attachment sites.

The synthetic route of ligand Fru-RGD-chol was illustrated in Scheme 1. Firstly, the C2,3,4,5-OH of D-fructose was protected by a propylidene group to obtain compound **2**. The C1–OH was extended by reacting with succinic anhydride to generate compound **3**. Secondly, the cholesterol derivative **6**, gained on the basis of our previous study [34], was conjugated with *N*-Boc-*N′*-Fmoc-L-lysine to obtain the intermediate **7** with two attachment sites. After that, compound **8** was generated by removing the Fmoc group, and immediately reacted with RGD derivative **21** (Scheme S1) to give compound **9** (NMM, IBCF, DCM). Similarly, compound **10** was generated by removing the Boc group, and it was further coupled with the fructose derivative **3** to obtain compound **11** (DIPEA, EDCI, DMAP). Finally, the protective group of fructose and RGD were removed by trifluoroacetic acid and $Pd/C/H_2$ respectively, to provide Fru-RGD-chol.

The synthetic route of ligand Fru-chol was illustrated in Scheme 2. Briefly, condensation of the fructose derivative **3** and the cholesterol derivative **6** gave compound **12** (DCC/DMAP). After deprotecting the propylidene groups, Fru-chol was gained. The synthesis of RGD-chol followed our previous work [28]. All the title compounds and important intermediates were characterized by their respective ^{1}H NMR and HRMS.

2.2. Preparation and characterization of liposomes

Liposomes were prepared by the thin film hydration method and the prescription followed previous work [28,35]. The characterizations of different liposomes in this study were listed in Table 1. The results showed that the entrapment efficiency (EE%) of these five PTX-loaded liposomes were greater than 80%, suggesting PTX was well loaded in liposomes. The particle sizes of the PTX-loaded liposomes were all around 110 nm, and the dispersity index (polymer dispersity index, PDI) was around 0.2, implying the liposomes were evenly distributed. Besides, the Zeta potential was weak negative electricity (about −5 mV), which can decrease the absorption of the reticuloendothelial system and immune response [36–38]. All of results contributed to achieve the passive targeting through the enhanced permeability and retention effect (EPR effect) [39,40].

2.3. In vitro stability of liposomes in serum

In order to reach the target site effectively and regulate the activity of loaded chemotherapeutic agents, the liposome must have a certain stability in the blood circulation. The turbidity method was used to monitor the stability of PTX-loaded liposomes in 50% fetal bovine serum (FBS) [41]. As Fig. 1 showed, after being incubated at 37 °C for 48 h, the transmittance of the five liposomes were still more than 90%. Besides, there was no obvious aggregation phenomenon, indicating that the prepared liposomes were stable in serum for a long time.

2.4. In vitro drug release study

The drug release properties were evaluated in phosphate buffer (PBS, pH 7.4) containing 0.1% Tween 80[41]. The results in Fig. 2 showed that the release of free paclitaxel was fastest, with more than 85% in 12 h and more than 90% in 48 h. The release of PTX in liposomes was much slower, about 70% within 48 h. In addition, there was no obvious burst release and significant difference in the release characteristics among the five liposomes. The data

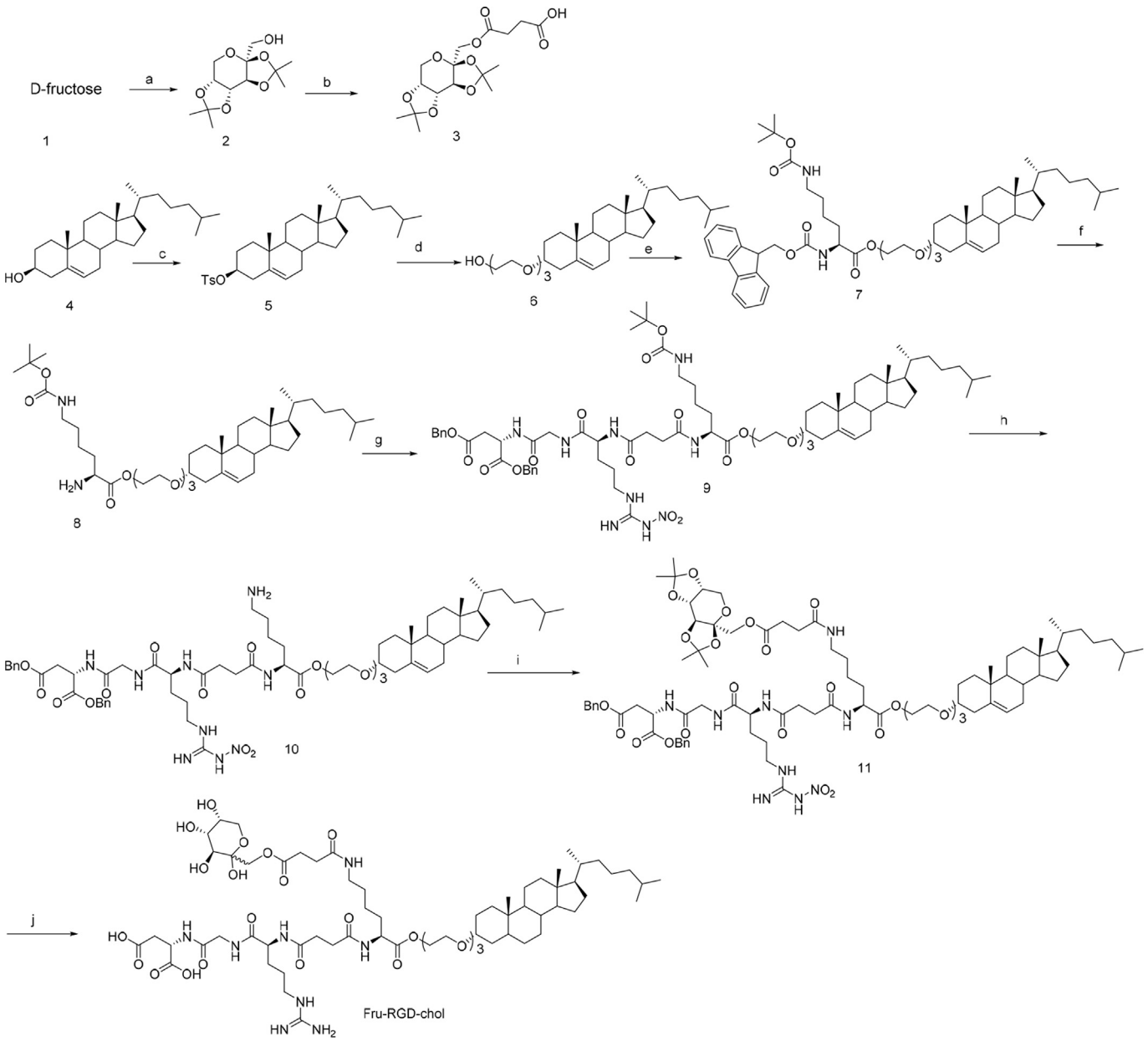

Scheme 1. Synthesis of ligand Fru-RGD-chol. Reagents and conditions: (a) 5% H_2SO_4-Acetone, 0 °C- r. t., 2 h, 73%; (b) Succinic anhydride, DMAP, Et_3N, toluene, 110 °C, 2.5 h, 97%; (c) TsCl, Pyridine, 0 °C−55 °C, overnight, 90%; (d) Triethylene glycol, dioxane, reflux, 6 h, 61%; (e) *N*-Boc-*N*′-Fmoc-L-lysine, DCC, DMAP, DCM, −5 °C- r. t., 8 h, 93%; (f) DBU, DCM, r. t., 20 min, 93%; (g) compound 21, NMM, IBCF, DCM, −5 °C- r. t., overnight, 81%; (h) TFA, DCM, r. t., 20 min, 99%; (i) compound 3, DIPEA, EDCI, DMAP, DCM, −5 °C- r. t., overnight, 77%; (j) TFA, H_2O, r. t., 24 h; then, H_2, Pd/C (10%), CH_3OH, 45 °C, 48 h.

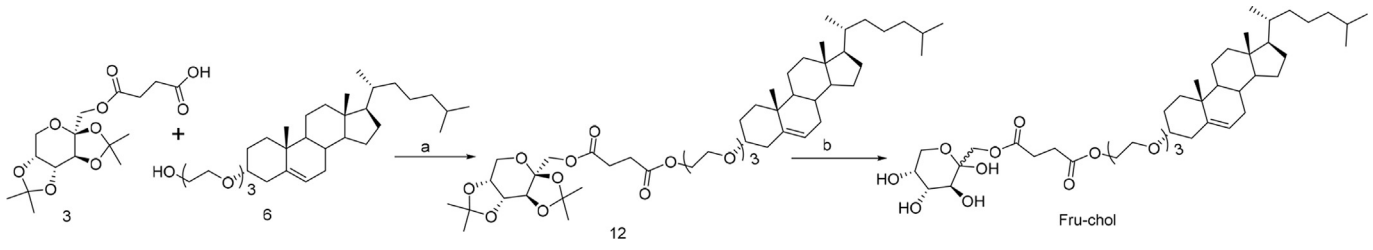

Scheme 2. Synthesis of ligand Fru-chol. Reagents and conditions: (a) DCC, DMAP, DCM, 0 °C- r. t., 3 h, 77%; (b) TFA, H_2O, r. t., 24 h, 38%.

Table 1
Particle sizes, zeta potentials and the PTX entrapment efficiency of five different PTX-loaded liposomes (n = 3, mean ± SD).

Liposomes	Size (nm)	PDI	EE (%)	Zeta potential (mV)
PTX-Lip	108.5 ± 4.7	0.203 ± 0.024	86.65 ± 1.53	−5.07 ± 0.14
PTX-Fru-Lip	108.8 ± 2.2	0.209 ± 0.017	81.47 ± 1.11	−4.54 ± 0.17
PTX-RGD-Lip	110.8 ± 6.2	0.198 ± 0.015	82.60 ± 2.09	−4.27 ± 0.24
PTX-Fru-RGD-Lip	112.0 ± 2.5	0.201 ± 0.019	82.16 ± 2.92	−4.74 ± 0.19
PTX-(Fru+RGD)-Lip	113.6 ± 2.1	0.186 ± 0.017	80.42 ± 3.02	−4.20 ± 0.17

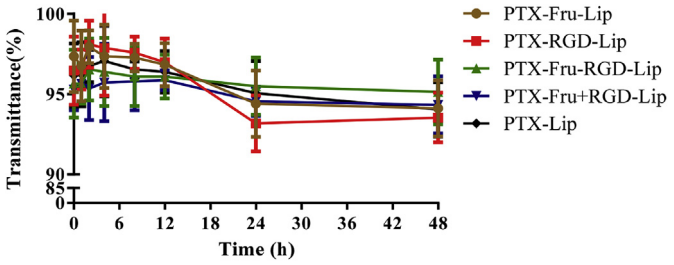

Fig. 1. Transmittance of PTX-Lip, PTX-Fru-Lip, PTX-RGD-Lip, PTX-Fru-RGD-Lip and PTX-Fru+RGD-Lip after incubation in 50% serum (n = 3, mean ± SD).

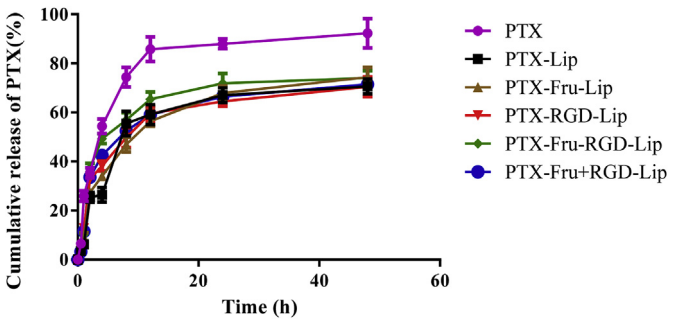

Fig. 2. *In vitro* drug release behavior of PTX-Lip, PTX-Fru-Lip, PTX-RGD-Lip, PTX-Fru-RGD-Lip, PTX-Fru+RGD-Lip and free PTX in PBS containing 0.1% Tween 80 within 48 h (n = 3, mean ± SD).

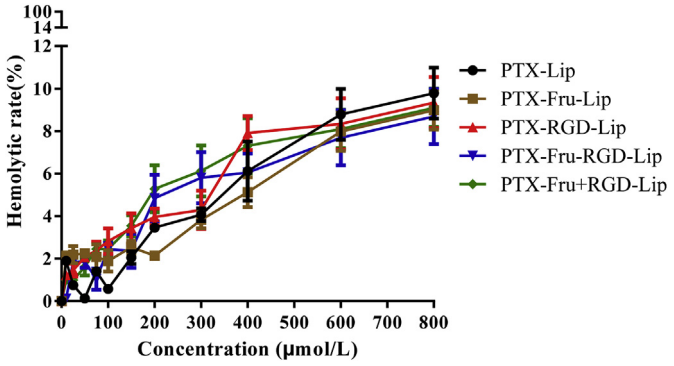

Fig. 3. Hemolysis rate of various concentrations of PTX-Lip, PTX-Fru-Lip, PTX-RGD-Lip, PTX-Fru-RGD-Lip and PTX-Fru+RGD-Lip (n = 3, mean ± SD).

indicated that the liposome can significantly improve the release behavior of the drug with a sustained release effect.

2.5. Hemolytic evaluation

The biosecurity of liposomes in the blood circulation is limited by hemocompatibility, so the hemolytic assay was conducted and the results were shown in Fig. 3. In the lipid concentration range of 10−800 μmol/L, the five liposomes did not cause significant hemoglobin release, and the hemolysis rate was less than 10%, which was regarded as non-toxic. All the characterizations indicated that the liposomes were fit for further *in vivo* and *in vitro* study.

2.6. Cytotoxicity

Cytotoxicity of different PTX-loaded liposomes on human triple-negative breast cancer cells (MDA-MB-231) [17,42] and murine triple-negative breast cancer cells (4T1) [17,43]overexpressing $GLUT_5$ and $\alpha_v\beta_3$ simultaneously, was evaluated by MTT assay. The results in Fig. 4A and B showed that PTX-Fru-RGD-Lip manifested the significant cytotoxicity compared to the other liposomes, with the highest inhibition of proliferation at each concentration. In addition, the group of free paclitaxel exhibited the lowest cell viability, probably because the free drugs could enter the cell through passive diffusion directly and take effect without a drug release process. The data further demonstrated the sustained release effect of the liposomes, which is consistent with the *in vitro* drug release study.

In order to further investigate the toxicity of the lipid material, the five types of blank liposomes were diluted to the corresponding concentration of the PTX-loaded liposomes. The result was shown in Fig. 4C and D. The unloaded lipid material showed no significant toxicity to cells even up to 800 μmol/L. At each lipid concentration, the cell viability was above 80%. Therefore, the unloaded lipid material was safe and nonvenomous to be further used *in vitro* and *in vivo*.

2.7. Cellular uptake

The CFPE-labeled liposomes were prepared to detect the liposomes entered cells. It can be seen from Fig. 5A and B, for MDA-MB-231 and 4T1 cells, Fru-RGD-Lip displayed the strongest cellular uptake, followed by Fru+RGD-Lip. The cellular uptake of Fru-RGD-Lip on MDA-MB-231 cells and 4T1 cells was 3.19- and 3.23-fold more than that of the uncoated liposomes (Lip). The uptake of Fru+RGD-Lip was slightly lower, giving a 2.81- and 2.90-fold increase than that of Lip in two cell lines, respectively.

The qualitative study by confocal laser scanning microscope (CLSM) in Fig. 5C and D was well consistent with the results of quantitative by flow cytometry. The target efficacy of the five different liposomes on both TNBC cells was Fru-RGD-Lip > Fru+RGD-Lip > RGD-Lip > Fru-Lip > Lip. In addition, the green fluorescence was mainly located in the cytoplasm, and the light blue fluorescent signal was rarely to be seen. The result indicated that the liposome was mainly located in the cytoplasm and rarely entered the nucleus, which was facilitating to the release of the drug after the phospholipid bilayer structure being destroyed under the acidic environment of the lysosome.

2.8. Uptake mechanism

In order to investigate the uptake mechanism of Fru-RGD-Lip

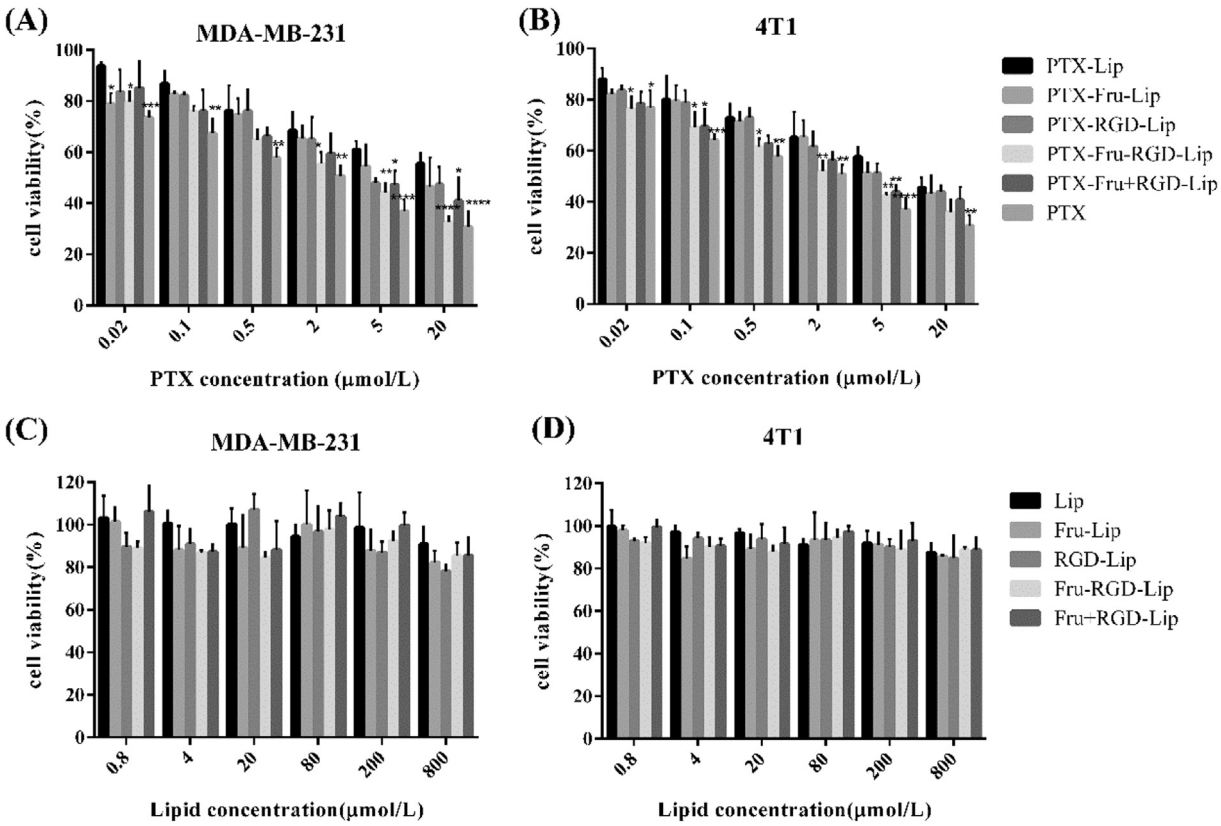

Fig. 4. The cytotoxicity of PTX-loaded liposomes on MDA-MB-231 cells (A) and 4T1 cells (B) for 24 h. The cytotoxicity of blank liposomes on MDA-MB-231 cells (C) and 4T1 cells (D) for 24 h (n = 3, mean ± SD; *P < 0.05, **P < 0.01, ***P < 0.001, ****P < 0.0001 versus PTX-Lip).

and Fru+RGD-Lip, receptor competition inhibitors and endocytosis inhibitors were used to explore the uptake mechanism study. It can be seen in Fig. 6 that both of free fructose and RGD can inhibit the cellular uptake of Fru-RGD-Lip and Fru+RGD-Lip to a certain extent, especially the fructose showed significant inhibition in the cellular uptake of Fru+RGD-Lip on 4T1 cells, whose relative cellular uptake was only 50.43%. Receptor competition studies proved that the cellular uptake of Fru-RGD-Lip and Fru+RGD-Lip was mediated by $GLUT_5$ and the integrin $\alpha_v\beta_3$. Chlorpromazine, filipin and amiloride hydrochloride [44–46] were chosen as the inhibitors of clathrin-mediated, caveolin-mediated and macropinocytosis endocytosis. For Fru-RGD-Lip, the cellular uptake was inhibited by the three inhibitors, while for Fru+RGD-Lip, only chlorpromazine and amiloride hydrochloride showed inhibition. Sodium azide and temperature can significantly affect the uptake of liposomes, especially the low temperature, the relative uptake rate dropped below 20%, indicating they were energy-dependent. In conclusion, the mechanism demonstrated that the cellular uptake of both dual-targeting liposomes was likely to be recognized and mediated by $GLUT_5$ and $\alpha_v\beta_3$, and endocytosed through comprehensive pathways with energy-dependent.

2.9. In vivo imaging

The tumor targeting ability of five liposomes *in vivo* was further investigated in a tumor-bearing mouse model established by subcutaneous inoculation of 1×10^6 cells in the right flank. The *in vivo* images of 4T1-bearing Balb/C were evaluated at different time points after systemic administration of DiD-labeled liposomes. As displayed in Fig. 7, DiD-Fru-RGD-Lip showed the strongest tumor targeting ability at each time point, followed by DiD-Fru+RGD-Lip. The single modified liposome DiD-Fru-Lip and DiD-RGD-Lip also improved a little compared to unmodified liposomes. The five liposomes reached the maximum accumulation in tumor at 12 h after injection, and the semi-quantitative data also showed the fluorescence intensity of DiD-Fru-RGD-Lip, DiD-Fru+RGD-Lip, DiD-Fru-Lip and DiD-RGD-Lip were 2.62, 1.85, 1.68 and 1.56 times of DiD-Lip respectively. After 24 h, the dual-targeting liposomes remaining at the tumor site were more than other groups. Moreover, the liposomes mainly accumulated in liver, the main metabolic organs, and reached the peak concentration at 6 h while most of them were eliminated at 24 h. And other organs were less enriched. These results indicated that the tumor targeting ability of the five liposomes was Fru-RGD-Lip > Fru+RGD-Lip > Fru-Lip > RGD-Lip > Lip, which was almost consistent with the *in vitro* targeting results.

It should be pointed out that the targeting ability of RGD-Lip and Fru+RGD-Lip didn't exhibit as excellent as *in vitro*, which may be that RGD-modified liposomes are more easily taken up by the liver [47–49], resulting in a slightly less enrichment at the tumor site. It can be proved that liposomes co-modified with fructose and RGD, especially covalently modified liposomes, can further significantly enhance the ability of liposomes to target TNBC based on singly modified liposomes. The improved targeting ability would efficiently enhance the therapeutic effect and reduce unwanted side effects to normal tissues.

3. Conclusion

Two types of novel dual-targeting TNBC liposomes (Fru-RGD-Lip and Fru+RGD-Lip) that actively recognize both fructose transporter $GLUT_5$ and integrin $\alpha_v\beta_3$ were designed and prepared in this work.

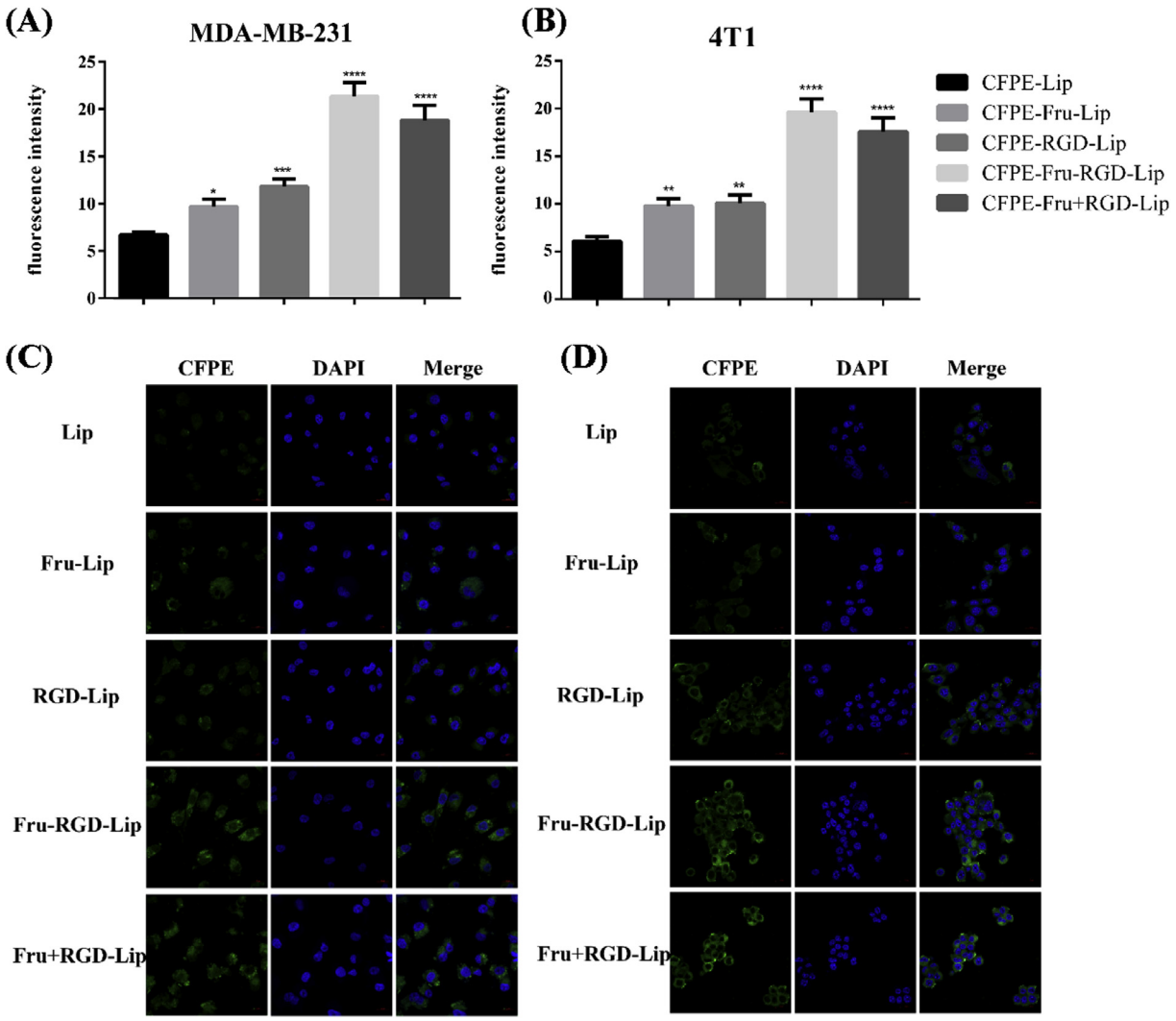

Fig. 5. Quantitative cellular uptake of CFPE-labeled liposomes on MDA-MB-231 cells (A) and 4T1 cells (B) determined by flow cytometer (n = 3, mean ± SD; *P < 0.05, **P < 0.01, ***P < 0.001, ****P < 0.0001 versus CFPE-Lip). Qualitative cellular uptake of CFPE-labeled liposomes on MDA-MB-231 cells (C) and 4T1 cells (D) determined by CLSM, green (CFPE-labeled liposomes), blue (DAPI stained nucleus), light blue (colocalized CFPE and DAPI). Scale bars represent 10 μm. (For interpretation of the references to color in this figure legend, the reader is referred to the Web version of this article.)

The dual-targeting liposomes were not only co-modified by Fru-chol and RGD-chol in a physical mixing manner (Fru+RGD-Lip), but also innovatively modified by the covalently linked Y-shaped Fru-RGD-chol ligand (Fru+RGD-Lip). Fru-RGD-Lip and Fru+RGD-Lip exhibited a variety of attractive properties such as improved cellular internalization, identified cellular uptake pathways, enhanced anti-proliferation effects on tumor cells, and surprisingly efficient accumulation at the tumor site. Besides, Fru-RGD-Lip showed much better targeting ability than Fru+RGD-Lip, making it a superior multifunctional liposome. Moreover, Fru-RGD-lip may also be applied to other tumors that overexpress GULT$_5$ and $\alpha_v\beta_3$. The idea of dual-targeting liposomes reported in this work could also provide new insight in the development of other novel targeted drug delivery system.

4. Experimental section

4.1. 1General

1,2-dioleoyl-sn-glycero-3-phosphoethanolamine-*N*-(carboxyfluorescein) (CFPE) were purchased from Avanti Polar Lipids (USA). 40-6-diamidino-2-pheylindole (DAPI) and 3-(4,5-Dimethylthiazol-2-yl)-2,5-diphenyltetrazolium bromide (MTT) were purchased from Beyotime Institute Biotechnology (Haimen, China). 1,1′-Dioctadecyl-3,3,3′,3′-tetramethyl indodicarbocyanine perchlorate (DiD) were purchased from Solarbio (Being, China). Sodium azide, amiloride, chlorpromazine and filipin were obtained from Sigma Aldrich (St. Louis, MO, USA). Paclitaxel (PTX)was obtained from National Institute for Food and Drug Control. All liquid reagents were distilled before use. The other chemicals and reagents were obtained from commercial sources. Kunming mice and Balb/C mice were purchased from Chengdu Dashuo Experimental Animal Co., Ltd (Chengdu, China).

The melting point was measured on a YRT-3 melting point apparatus (Shantou Keyi Instrument & Equipment Co. Ltd., Shantou, China). ^{1}H NMR spectra were taken on a Varian INOVA 400 or 600 (Varian, Palo Alto, CA) using CD_3Cl and CD_3OD as solvent. High-resolution mass spectroscopy data of the product were collected on a Waters Micromass GCT or a Bruker Apex IV FTMS instrument. Optical rotation was obtained from Rudolph Research Analytical Autopol VI automatic polarimeter. Reversed-phase chromatography performed on C18 chromatographic analysis was carried out

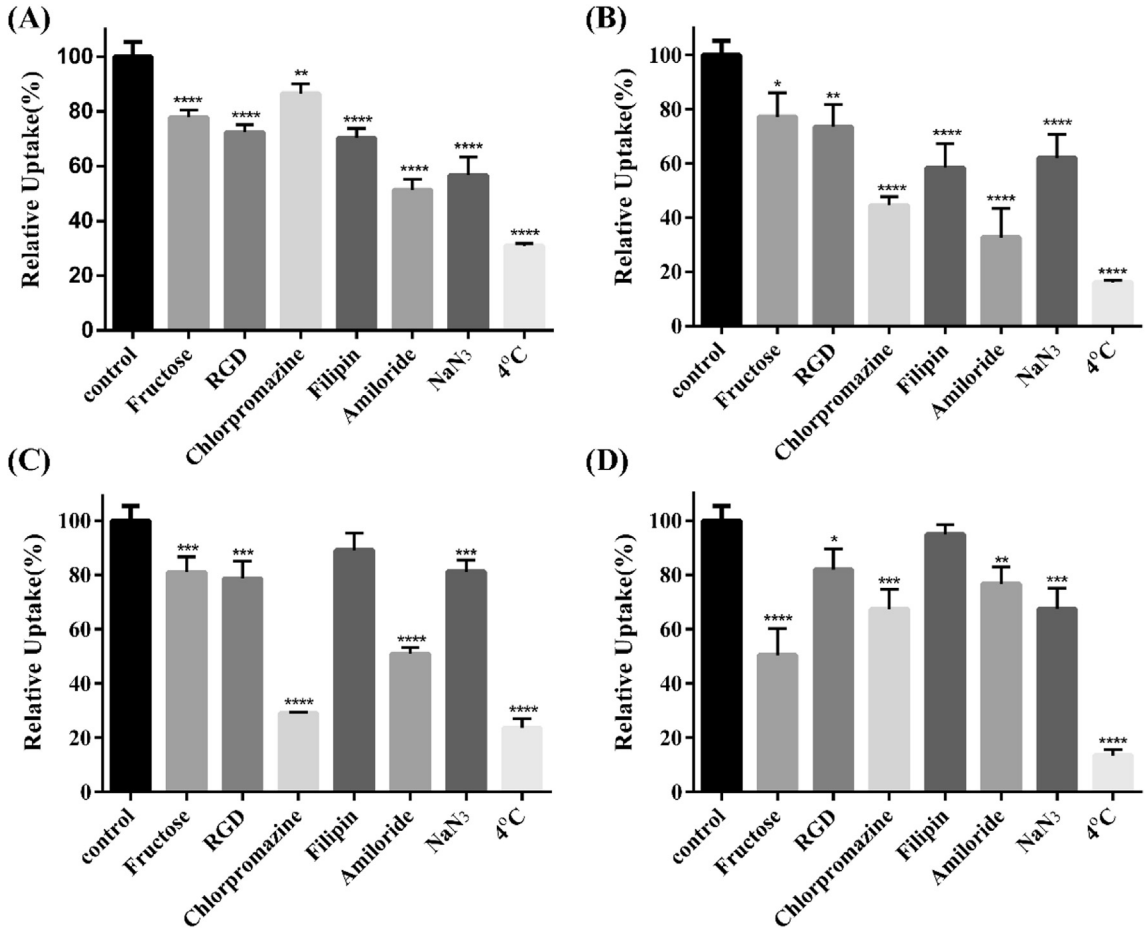

Fig. 6. The relative uptake of CFPE-Fru-RGD-Lip on MDA-MB-231 cells (A) and 4T1 cells (B); The relative uptake of CFPE-Fru+RGD-Lip on MDA-MB-231 cells (C) and 4T1 cells (D). (mean ± SD, n = 3; *P < 0.05, **P < 0.01, ***P < 0 0.001, ****P < 0.0001 versus control).

using the high-performance liquid chromatography (HPLC) system (Shimadzu, Kyoto, Japan). Particle size and potential were determined using Sizer Nano ZS90 laser particle size and Zeta potential analysis (Malvern, UK). Cellular uptake was detected by flow cytometry (BD FACS Celesta, USA) and laser confocal microscopy (Carl Zeiss LSM800, Germany); *in vivo* imaging experiment was conducted by small animal *in vivo* imager (PerkinElmer IVIS Lumina III, USA).

4.2. Chemistry

4.2.1. Synthesis of compound **2**

The anhydrous D-fructose **1** (2.00 g, 11.11 mmol) was added to a mixed solution of anhydrous acetone (39 mL) and sulfuric acid (1.95 mL) at 0 °C. And the reaction solution was stirred at room temperature (r.t.) for 2 h. Then, the mixture was neutralized by aqueous sodium hydroxide (0.10 g, 152 mmol, 55 mL) and filtered. The filtrate was concentrated and re-dissolved in CH_2Cl_2 (100 mL), followed by washed with H_2O (100 mL × 2) and saturated NaCl (100 mL × 3). The organic layer was dried over anhydrous Na_2SO_4 and concentrated. The residue was purified by recrystallized with petroleum ether to give **2** as a white solid (2.10 g, 73%). Mp: 94–96 °C (literature Mp [50]: 95–96 °C). [a]$_{20}^{D}$: −22.0 (c 0.5, $CHCl_3$).

4.2.2. Synthesis of compound **3**

Compound **2** (2.00 g, 7.69 mmol), succinic anhydride (923 mg, 9.23 mmol) and 4-dimethylaminopyridine (DMAP, 94 mg, 0.77 mmol) were dissolved in a mixed solution of toluene (30 mL) and triethylamine (1 mL) under argon. And the reaction was refluxed at 110 °C for 2.5 h. Then, toluene was removed, and the residue was dissolved in a mixture of CH_2Cl_2 (38 mL) and H_2O (54 mL), and pH was adjusted to neutral with acetic acid. The mixture was extracted with CH_2Cl_2 (40 mL × 3), and the organic phase was concentrated to give **3** as a colorless oil (2.69 g, 97%). ^{1}H NMR (600 MHz, $CDCl_3$, ppm) δ: 1.34 (s, 3H), 1.41 (s, 3H), 1.48 (s, 3H), 1.54 (s, 3H), 2.70 (s, 4H), 3.75–3.78 (m, 1H), 3.89–3.92 (m, 1H), 4.06–4.09 (m, 1H), 4.23–4.25 (m, 1H), 4.31 (s, 1H), 4.42–4.45 (m, 1H), 4.60–4.61 (m, 1H). [a]$_{20}^{D}$: −23.0 (c 0.5, $CHCl_3$).

4.2.3. Synthesis of compound **5**–**6**

The synthesis of compound **5**–**6** was reported in our previous work [34].

4.2.4. Synthesis of compound **7**

To a solution of *N*-Boc-*N*′-Fmoc-L-lysine (5.00 g, 10.67 mmol) in CH_2Cl_2 (25 mL), was added dicyclohexylcarbodiimide (DCC, 2.93 g, 14.23 mmol) and DMAP (174 mg, 1.42 mmol), and the reaction was stirred at −5 °C for 30 min. Then a solution of compound **6** (3.69 g, 7.11 mmol) in CH_2Cl_2 (5 mL) was slowly added dropwise to the reaction. The reaction was stirred at r. t. for 8 h. After the by-product was filtrated and the filtrate was concentrated, compound **7** was obtained by silica gel column chromatography (petroleum/Acetone = 8/1) as a pale yellow solid (6.41 g, 93%).^{1}H NMR

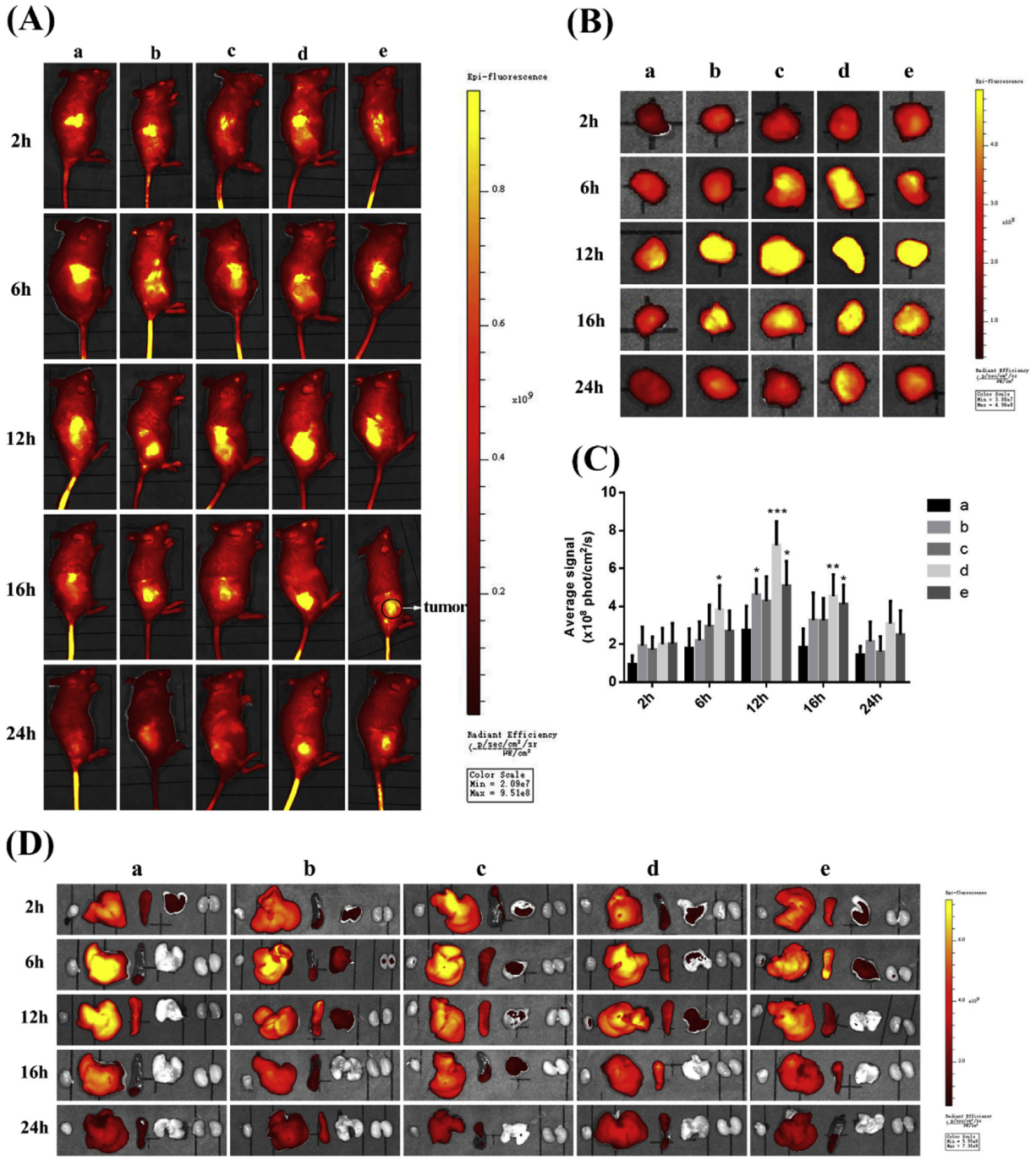

Fig. 7. (A) *In vivo* images of the 4T1-bearing Balb/C mice at 2 h, 6 h, 12 h, 16 h and 24 h after systemic administration of DiD-labeled liposomes. (B) *Ex vivo* images of tumors. (C) Semi-quantitative fluorescence intensity of isolated tumors; (D) *Ex vivo* images of isolated organs, and they were heart, liver, spleen, lung and kidney from left to right. (a = DiD-Lip, b = DiD-Fru-Lip, c = DiD-RGD-Lip, d = DiD-Fru-RGD-Lip, e = DiD-Fru+RGD-Lip. n = 3, mean ± SD; *P < 0.05, **P < 0.01, ***P < 0.001, ****P < 0.0001.)

(400 MHz, $CDCl_3$, ppm) δ: 0.67 (s, 3H), 0.86 (d, 6H, J = 6.4 Hz), 0.91 (d, 3H, J = 6.4 Hz), 0.98 (s, 3H), 1.43 (s, 9H), 0.85–2.36 (remaining cholesterol & Lys protons), 3.10–3.19 (m, 3H), 3.62–3.64 (m, 8H), 3.71 (t, 2H, J = 4.6 Hz), 4.22 (t, 1H, J = 6.8 Hz), 4.30–4.31 (m, 2H), 4.35–4.44 (m, 3H), 5.32–5.33 (m, 1H), 7.32 (t, 2H, J = 7.2 Hz), 7.40 (t, 2H, J = 7.2 Hz), 7.61 (d, 2H, J = 7.2 Hz), 7.77 (d, 2H, J = 7.2 Hz). HRMS (ESI) calculated for $C_{59}H_{88}N_2NaO_9^+$ $[M+Na]^+$-991.6382, found 991.6388. [a $]_{20}^{D}$: −12.6 (c 0.5, $CHCl_3$).

*4.2.5. Synthesis of compound **8***

To a solution of compound **7** (2.58 g, 2.66 mmol) in CH_2Cl_2 (20 mL) was added 1,8-diazabicycloundec-7-ene (DBU, 1.194 mL, 7.98 mmol), and the reaction was stirred at r. t. for 20 min. The mixture was washed with H_2O (50 mL × 3) and saturated NaCl (100 mL × 2) successively, and the organic layer was concentrated and purified by silica gel column chromatography (CH_2Cl_2/CH_3OH = 15/1) to give compound **8** as a pale yellow solid (1.85 g, 93%).^{1}H NMR (400 MHz, $CDCl_3$, ppm) δ: 0.67 (s, 3H), 0.86 (d, 6H,

$J = 6.4$ Hz), 0.91 (d, 3H, $J = 6.4$ Hz), 0.99 (s, 3H), 1.43 (s, 9H), 0.85–2.38 (remaining cholesterol & Lys protons), 3.12–3.21 (m, 3H), 3.63–3.66 (m, 8H), 3.70–3.75 (m, 4H), 4.14–4.15 (m, 1H), 4.31–4.43 (m, 2H), 5.34 (s, 1H), 8.69 (s, 2H). [a]$^{D}_{20}$: −7.6 (c 0.5, $CHCl_3$).

4.2.6. Synthesis of compound **9**

4-methylmorpholin (NMM, 0.127 mL, 1.15 mmol) and isobutyl chloroformate (IBCF, 0.151 mL, 1.15 mmol) were added to a solution of compound **8** (900 mg, 1.34 mmol) in CH_2Cl_2 (10 mL), and the reaction was stirred at −5 °C for 30 min. Then, a solution of compound **21** (715 mg, 0.96 mmol) in CH_2Cl_2 (10 mL), was slowly added dropwise. The reaction was stirred at r. t. overnight. The mixture was washed with hydrochloric acid (1 N, 50 mL × 2) and saturated NaCl (50 mL × 2). The organic layer was concentrated and purified by silica gel column chromatography ($CH_2Cl_2/CH_3OH = 50/1$) to give compound **9** as a pale yellow foamy solid (1.09 g, 81%). ^{1}H NMR (400 MHz, $CDCl_3$, ppm) δ: 0.67 (s, 3H), 0.86 (d, 6H, $J = 6.4$ Hz), 0.91 (d, 3H, $J = 6.4$ Hz), 0.98 (s, 3H), 1.41 (s, 9H), 0.85–2.37 (remaining cholesterol & Lys protons & Arg protons), 2.54 (s, 4H), 2.78 (br, 2H), 3.05 (s, 2H), 3.13–3.21 (m, 1H), 3.29 (s, 2H), 3.61–3.63 (m, 8H), 3.67 (s, 2H), 3.93 (s, 2H), 4.19–4.28 (m, 2H), 4.44 (s, 2H), 4.91 (br, 1H), 5.04 (s, 2H), 5.09–5.10 (m, 2H), 5.32–5.33 (m, 1H), 7.25–7.33 (m, 10H). [a]$^{D}_{20}$: −6.2 (c 0.5, $CHCl_3$).

4.2.7. Synthesis of compound ***10***

Compound **9** (1.092 g, 0.78 mmol) was added to a mixture of trifluoroacetic acid (TFA, 3 mL) and CH_2Cl_2 (9 mL), and the reaction was stirred at r. t. for 20 min. The solvent was removed and the residue was re-dissolved with CH_2Cl_2 (50 mL), followed by washed with H_2O (50 mL × 1), saturated $NaHCO_3$ (50 mL × 1), and saturated NaCl (50 mL × 2). The organic layer was concentrated to give compound **10** as a light yellow solid (0.999 g, 99%). ^{1}H NMR (400 MHz, $CDCl_3$, ppm) δ: 0.67 (s, 3H), 0.86 (d, 6H, $J = 6.4$ Hz), 0.91 (d, 3H, $J = 6.4$ Hz), 0.98 (s, 3H), 0.86–2.36 (remaining cholesterol & Lys protons & Arg protons), 2.56 (br, 4H), 2.94–3.20 (m, 5H), 3.27 (s, 2H), 3.62–3.65 (m, 10H), 3.92 (br, 2H), 4.25 (s, 2H), 4.42–4.55 (m, 2H), 4.90 (br, 1H), 5.04–5.09 (m, 4H), 5.33 (s, 1H), 7.28–7.32 (m, 10H). [a]$^{D}_{20}$: −6.2 (c 0.5, CH_3OH).

4.2.8. Synthesis of compound ***11***

To a solution of compound **3** (415 mg, 1.15 mmol) in CH_2Cl_2 (10 mL), were added *N*,*N*-diisopropylethylamine (DIPEA, 0.38 mL, 2.30 mmol), 1-(3-dimethylaminopropyl) 3-ethylcarbodiimide hydrochloride (EDCI, 294 mg, 1.54 mmol) and DMAP (188 mg, 1.54 mmol), and the reaction was stirred at −5 °C for 30 min. A solution of compound **10** (999 mg, 0.77 mmol) in CH_2Cl_2 (10 mL) was added dropwise, and the mixture was stirred at r. t. overnight. The mixture was washed with HCl solution (1 N, 30 mL × 2) and saturated NaCl (30 mL × 2). The organic layer was concentrated, and the residue was purified by silica gel column chromatography $CH_2Cl_2/CH_3OH = 8/1$) to give compound **11** as a white foamy solid (977 mg, 77%). ^{1}H NMR (400 MHz, CDCl [3], ppm) δ: 0.67 (s, 3H), 0.86 (d, 6H, $J = 6.6$ Hz), 0.91 (d, 3H, $J = 6.2$ Hz), 0.98 (s, 3H), 1.33 (s, 3H), 1.39 (s, 3H), 1.46 (s, 3H), 1.52 (s, 3H), 0.86–2.36 (remaining cholesterol & Lys protons & Arg protons), 2.51–2.75 (m, 8H), 2.90–3.06 (m, 2H), 3.13–3.33 (m, 5H), 3.62–3.64 (m, 8H), 3.66–3.69 (m, 2H), 3.72–3.76 (m, 1H), 3.87–3.93 (m, 3H), 3.99–4.02 (m, 1H), 4.22–4.26 (m, 3H), 4.30–4.31 (m, 1H), 4.42–4.47 (m, 3H), 4.59–4.61 (m, 1H), 4.88–4.91 (m, 1H), 5.02–5.14 (m, 4H), 5.33 (s, 1H), 7.28–7.34 (m, 10H). HRMS (ESI) calculated for $C_{85}H_{127}N_9NaO^{+}_{23}$ $[M+Na]^+$-1664.8937, found 1664.8939. Mp: 46–48 °C.[a]$^{D}_{20}$: −6.0 (c 0.5, $CHCl_3$).

4.2.9. Synthesis of compound Fru-RGD-chol

Compound **11** (100 mg, 0.06 mmol) was added to a mixed solvent of TFA (3 ml) and H_2O (3 ml), and the reaction was stirred at r. t for 24 h. Then TFA was removed, and the residue was diluted with water and extracted with CH_2Cl_2 (30 mL × 3). The organic layer was washed with saturated NaCl (30 mL × 2) and concentrated to give a pale yellow semi-solid (86 mg). The pale yellow semi-solid was further dissolved in of methanol (10 mL), and 10% Pd/C (10 mg) was added. The reaction was stirred under a hydrogen pressure (0.4 Mpa) at 45 °C for 48 h. Then, Pd/C was removed by filtration, and the solvent in filtrate was removed. The residue was washed with diethyl ether (5 mL × 5) to remove the small polar impurity (10 mL × 5) to give a white solid (21.86 mg). ^{1}H NMR (400 MHz, CD_3OD, ppm) δ: 0.67 (s, 3H), 0.86 (d, 6H, $J = 6.8$ Hz), 0.91 (d, 3H, $J = 6.4$ Hz), 0.98 (s, 3H), 0.86–2.37 (remaining cholesterol and Lys protons), 2.50–2.79 (m, 10H), 2.90–3.05 (m, 2H), 3.17–3.20 (m, 2H), 3.62–3.76 (m, 12H), 3.77–3.94 (m, 5H), 4.18–4.35 (m, 8H), 4.61 (br, 1H). HRMS (ESI) calculated for $C_{66}H_{110}N_8NaO^{+}_{21}$ $[M^+Na]^+$-1361.7678, found 1361.7674.

4.2.10. Synthesis of compound ***12***

To a solution of compound **3** (1.04 g, 2.89 mmol) in CH_2Cl_2 (30 mL), were added DCC (795 mg, 3.86 mmol) and DMAP (47 mg, 0.39 mmol), and the reaction was stirred at −5 °C for 30 min. A solution of compound **6** (1.00 g, 1.93 mmol) in CH_2Cl_2 (20 mL) was added dropwise and the reaction was stirred at r. t for 3 h. The solvent was removed, and the residue was re-dissolved by ethyl acetate (50 mL), and then filtrated. The filtrate was concentrated and purified by silica gel column chromatography (petroleum ether/ethyl acetate = 5/1) to give compound **12** as a pale yellow viscous oil (1.78 g, 77%). ^{1}H NMR (400 MHz, $CDCl_3$, ppm) δ: 0.67 (s, 3H), 0.86 (d, 6H, $J = 6.4$ Hz), 0.91 (d, 3H, $J = 6.4$ Hz), 0.99 (s, 3H), 1.34 (s, 3H), 1.41 (s, 3H), 1.48 (s, 3H), 1.54 (s, 3H), 0.86–2.39 (remaining cholesterol protons), 2.69 (s, 4H), 3.14–3.22 (m, 1H), 3.64–3.66 (m, 8H), 3.69–3.72 (m, 2H), 3.75–3.78 (m, 1H), 3.89–3.93 (m, 1H), 4.05–4.08 (m, 1H), 4.23–4.27 (m, 3H), 4.31 (d, 1H, $J = 2.6$ Hz), 4.42–4.44 (m, 1H), 4.59–4.62 (m, 1H), 5.34 (s, 1H). HRMS (ESI) calculated for $C_{49}H_{80}O_{12}Na^+$ $[M+Na]^+$-883.5542, found 883.5550. [a]$^{D}_{20}$: −17.6 (c 0.5, $CHCl_3$).

4.2.11. Synthesis of Fru-chol

Compound **12** (3.49 g, 4.00 mmol) was added to a mixed solvent of TFA (20 mL) and H_2O (20 mL), and the reaction was stirred at r. t. for 24 h. The TFA was removed, then the mixture was neutralized with Na_2CO_3, and extracted by Ethyl acetate (50 mL × 3). The organic layer was concentrated and purified by silica gel column chromatography (petroleum ether/ethyl acetate = 3/1) to give a pale yellow viscous oil (1.197 g, 38%).^{1}H NMR (400 MHz, $CDCl_3$, ppm) δ: 0.67 (s, 3H), 0.86 (d, 6H, $J = 6.4$ Hz), 0.91 (d, 3H, $J = 6.4$ Hz), 1.00 (s, 3H), 0.86–2.38 (remaining cholesterol protons), 2.68 (s, 4H), 3.16–3.21 (m, 1H), 3.42–3.50 (m, 7H), 3.62–3.69 (m, 10H), 4.25–4.36 (m, 4H), 5.34 (s, 1H). HRMS (ESI) calculated for $C_{43}H_{72}NaO^{+}_{12}$[M+Na]$^+$- 803.4916, found 803.4912.

4.3. Preparation and characterization of liposomes

We selected the optimal prescription: cholesterol: soybean phospholipid (SPC): ligand = 33:64:3 (molar ratio), and lipid: paclitaxel = 30:1 (quality ratio), hydration solution was PBS (pH = 7.4). Briefly, the prescribed amount of lipid material and PTX were accurately weighed to be dissolved with chloroform-methanol mixed solution (V/V = 2/1). And then the organic solvent was removed by rotary evaporation at 37 °C to give a complete thin film. The thin film was hydrated in PBS for 0.5 h at 20 °C. Finally, it was further sonicated intermittently (80 W, 5S, 5S) for

3 min to give slightly milky liposome solution. Likewise, CFPE-labeled liposomes or DiD-labeled liposomes were prepared with appropriate amount of CFPE or DiD added to the solution before removing the solvent.

The encapsulation efficiency of PTX-loaded liposomes was detected by HPLC after the unencapsulated free paclitaxel and PTX-loaded liposomes were separated by cryo-centrifugation [51]. The encapsulation efficiency (EE%) of the PTX-loaded liposome was calculated according to the formula: $EE\% = A_{\text{after centrifugation}}/A_{\text{before centrifugation}} \times 100\%$. After the prepared liposome was diluted to a suitable concentration with ultrapure water, the particle size and zeta potential of the liposome were measured by Malvern Zeta sizer Nano ZS90.

4.4. In vitro drug release study

In vitro drug release of different PTX-loaded liposomes was investigated by dialysis method. 0.4 mL PTX-loaded liposomes or free PTX were placed in a dialysis bag of 8000−12000 Da. Then, the dialysis bag was sealed tightly and placed in 40 mL dialysis medium (1% Tween 80 in PBS, v/v). After being incubated at 37 °C with gently waggling, 0.1 ml release medium of each group was taken out at 0 h, 0.5 h, 1 h, 2 h, 4 h, 8 h, 12 h, 24 h and 48 h, to be analyzed by HPLC as the previous work described [28].

4.5. In vitro stability of liposomes in serum

Each group of PTX-loaded liposomes were mixed with an equal volume of FBS and co-incubated at 37 °C. Then, the transmittance of the sample was measured at 0 h, 1 h, 2 h, 4 h, 8 h, 12 h, 24 h and 48 h by a microplate reader at 750 nm. The control group was determined by the transmittance measured immediately after the liposomes were mixed with the PBS, whose transmittance was regarded as 100%.

4.6. Hemolysis assays

The blood of 18−22 g Kunming mice was taken from the eyelids and collected in a centrifuge tube coated with heparin sodium, and centrifuged at 4 °C (10000 rpm × 10 min) to discard the supernatant. And then the red blood cells (RBCs) were washed with PBS until the supernatant was colorless. Subsequently, the RBCs were resuspended in PBS to the concentration of 2% (w/v). The PTX-loaded liposomes were gradually diluted with PBS to give lipid concentrations of 800, 400, 300, 200, 150, 75, 50, 25, 10 μmol/L. Finally, various concentrations of liposomes were co-incubated with an equal volume of 2% RBCs at 37 °C for 1 h. After being centrifuged at 10,000 rpm for 10 min, the absorbance of the supernatant was detected with a microplate reader at 540 nm. The positive control and the negative control were determined by co-incubation of RBCs with 1% Triton X-100 and PBS, whose hemolysis rate was set to 100% and 0% respectively. The hemolysis rate of each group of liposomes was calculated as: percent hemolysis $\% = (A_{\text{sample}} - A_{\text{negative}})/(A_{\text{positive}} - A_{\text{negative}}) \times 100\%$.

4.7. Cytotoxicity

MDA-MB-231 cells or 4T1 cells were seeded in a 96-well plate at a density of 5×10^3 cells/well, and cultured for 24 h at 37 °C. The PTX-loaded liposomes or free PTX were diluted to a PTX concentration of 20, 5, 2, 0.5 0.1 and 0.02 μmol/L, and added to the plates. After being incubated for 24 h, the medium was discarded and replaced by 200 μL of serum-free medium containing MTT (0.5 mg/mL), and the plates were further incubated for 4 h. Finally, the medium was removed, and the reduced MTT dye was solubilized by DMSO (150 μl). The optical density absorption value (OD) was measured at 570 nm. The cell survival rate was calculated as: cell Viability $(\%) = OD_{\text{sample}}/OD_{\text{control}} \times 100\%$. The OD_{control} and OD_{sample} represented the value of the cells treated with blank medium and various drugs, respectively.

4.8. Cellular uptake

MDA-MB-231 cells and 4T1 cells were seeded in a 12-well plate at a density of 1×10^5 cells/well and 2×10^5 cells/well respectively, and cultured to reach 80% confluence. The CFPE-labeled liposomes were added with a lipid concentration at 0.3 μmol/mL and a CFPE concentration at 2 μg/mL. After being incubated for 2 h, the cells were washed twice with pre-cooled PBS, followed by trypsinized and collected. Finally, the cells were resuspended in PBS, and the fluorescence intensity was measured by flow cytometry.

For confocal microscope studies, MDA-MB-231 and 4T1 cells were seeded at a density of 5×10^5 or 1×10^6 cells/well in a 6-well plate pre-coated with cover glasses, and cultured for 24 h. Then, CFPE-labeled liposomes were added to incubate for 2 h. After that, cells were fixed with 4% paraformaldehyde for 30 min and stained with 5 μg/mL DAPI for 5 min. The samples were sealed with glycerin and imaged with a laser confocal microscope.

4.9. Uptake mechanism

In order to illuminate the uptake mechanism of Fru-RGD-Lip and Fru+RGD-Lip, MDA-MB-231 cells and 4T1 cells were pre-incubated with receptor competition inhibitors (10 g/L fructose or 200 μg/mL RGD), endocytosis inhibitors (10 μg/mL chlorpromazine, 1 μg/mL filipin or 2 mg/mL amiloride hydrochloride), and energy inhibitor (1 mg/mL NaN_3) at 37 °C for 30 min. Then, the CFPE-labeled liposomes were added to incubate for another 2 h. The low temperature group was set up, which was incubated for 2 h at 4 °C. Finally, the cells were treated as described in 4.8 and measured by flow cytometry.

4.10. In vivo imaging

4T1 cells were injected into female Balb/C mice to establish a tumor model. After 14 days, the mice were given DiD-labeled liposomes through tail vein injection at a dose of 500 μg/kg DiD. After administration of 2 h, 6 h, 12 h, 16 h and 24 h, each group of mice were anesthetized with 4% chloral hydrate and imaged with IVIS Lumina Series III imaging system. And then, the heart, liver, spleen, lung, kidney and tumor were taken out immediately after the mice were sacrificed by heart perfusion, and also imaged. The average fluorescence intensity of the *ex vivo* tumors were calculated by the Image software.

4.11. Statistical analysis

Data was analyzed by the Graphpad Prism 6 software. Statistical comparisons were performed by one-way ANOVA for multiple groups. The results were analyzed by student's *t*-test. Significant differences between or among groups were indicated by $^*P < 0.05$, $^{**}P < 0.01$, $^{***}P < 0.001$, $^{****}P < 0.0001$.

Acknowledgement

This work was supported by the National Natural Science Foundation of China (No. 81573286, & No. 81773577 & No.81903448); the Sichuan Science and Technology Program (2018JY0537); the Sichuan Youth Science and Technology Innovation Research Team Funding (2016TD0001); the Fundamental

Research Funds for the Central Universities (2012017yjsy211); and the Open Research Subject of Healthy, Xihua University (szjj2017-036).

Appendix A. Supplementary data

Supplementary data to this article can be found online at https://doi.org/10.1016/j.ejmech.2019.111720.

References

[1] A.M. Brewster, C.M. Mariana, B. Powel, Epidemiology, biology, and treatment of triple-negative breast cancer in women of African ancestry, Lancet Oncol. 15 (13) (2014) 625–634, https://doi.org/10.1016/S1470-2045(14)70364-X.

[2] J.S. Reis-Filho, A.N.J. Tutt, Triple negative tumours: a critical review, Histopathology 52 (1) (2010) 108–118, https://doi.org/10.1111/j.1365-2559.2007.02889.x.

[3] E.A. Rakha, I.O. Ellis, Triple-negative/basal-like breast cancer: review, Pathology 41 (1) (2009) 40–47, https://doi.org/10.1080/00313020802563510.

[4] O. Catherine, V. Giuseppe, D.L. Angelo, Management of triple negative breast cancer, Breast 19 (5) (2010) 312–321, https://doi.org/10.1016/j.breast.2010.03.026.

[5] A.J. Primeau, R. Augusto, H. David, L. Lothar, I.F. Tannock, The distribution of the anticancer drug Doxorubicin in relation to blood vessels in solid tumors, Clin. Cancer Res. 11 (1) (2005) 8782–8788, https://doi.org/10.1158/1078-0432.CCR-05-1664.

[6] E. Bernabeu, L. Gonzalez, M. Cagel, E.P. Gergic, M.A. Moretton, D.A. Chiappetta, Novel Soluplus(®)-TPGS mixed micelles for encapsulation of paclitaxel with enhanced in vitro cytotoxicity on breast and ovarian cancer cell lines, Colloids Surfaces B Biointerfaces 140 (2016) 403–411, https://doi.org/10.1016/j.colsurfb.2016.01.003.

[7] A.S. Abu Lila, T. Ishida, Liposomal delivery systems: design optimization and current applications, Biol. Pharm. Bull. 40 (1) (2017) 1–10, https://doi.org/10.1248/bpb.b16-00624.

[8] S. Huaming, N. Ben, S. Hongbin, Metabolic targeting of cancers: from molecular mechanisms to therapeutic strategies, Curr. Med. Chem. 16 (13) (2009) 1561–1587, https://doi.org/10.2174/092986709788186255.

[9] X.D. Xu, S.X. Shao, H.P. Jiang, Y.W. Cao, Y.H. Wang, X.C. Yang, Y.L. Wang, X.S. Wang, H.T. Niu, Warburg effect or reverse Warburg effect? A review of cancer metabolism, Oncol. Res. Treat. 38 (3) (2015) 117–122, https://doi.org/10.1159/000375435.

[10] G. Gayatri, Z.K. Sabine, J. Anitha, R. Robert, L. Jelena, S. Ananth, B.J. Kjerstin, C. John, D. Ludger, S.S. Gambhir, GLUT5 is not over-expressed in breast cancer cells and patient breast cancer tissues, PLoS One 6 (11) (2011) 26902–26909, https://doi.org/10.1371/journal.pone.0026902.

[11] B.J. Trayner, T.N. Grant, F.G. West, C.I. Cheeseman, Synthesis and characterization of 6-deoxy-6-fluoro-d-fructose as a potential compound for imaging breast cancer with PET, Bioorg. Med. Chem. 17 (15) (2009) 5488–5495, https://doi.org/10.1016/j.bmc.2009.06.034.

[12] S.P. Zamora-León, D.W. Golde, I.I. Concha, C.I. Rivas, F.,. Delgado-López, J.,. Baselga, F.,. Nualart, J.C. Vera, Expression of the fructose transporter GLUT5 in human breast cancer, Proc. Natl. Acad. Sci. U.S.A. 93 (5) (1996) 1847–1852, https://doi.org/10.2307/38426.

[13] C.A. Colville, M.J. Seatter, T.J. Jess, G.W. Gould, H.M. Thomas, Kinetic analysis of the liver-type (GLUT2) and brain-type (GLUT3) glucose transporters in Xenopus oocytes: substrate specificities and effects of transport inhibitors, Biochem. J. 290 (Pt3) (1993) 701–706, https://doi.org/10.1111/j.1745-4603.1989.tb00424.x.

[14] T.,. Kayano, C.F. Burant, H.,. Fukumoto, G.W. Gould, Y.S. Fan, R.L. Eddy, M.G. Byers, T.B. Shows, S. Seino, G.I. Bell, Human facilitative glucose transporters. Isolation, functional characterization, and gene localization of cDNAs encoding an isoform (GLUT5) expressed in small intestine, kidney, muscle, and adipose tissue and an unusual glucose transporter pseudogene-like, J. Biol. Chem. 265 (22) (1990) 13276–13282, https://doi.org/10.0000/PMID1695905.

[15] A.R. Manolescu, K. Witkowska, A. Kinnaird, T. Cessford, C. Cheeseman, Facilitated hexose transporters: new perspectives on form and function, Physiology 22 (4) (2007) 234–240, https://doi.org/10.1152/physiol.00011.2007.

[16] I. Stuart W, T. Paul, Glucose transporters (GLUT and SGLT): expanded families of sugar transport proteins, Br. J. Nutr. 89 (1) (2003) 3–9, https://doi.org/10.1079/BJN2002763.

[17] X. Fan, H. Liu, M. Liu, Y. Wang, L. Qiu, Y. Cui, Increased utilization of fructose has a positive effect on the development of breast cancer, Peerj 5 (2) (2017) 3804–3818, https://doi.org/10.7717/peerj.3804.

[18] G. Alejandro, U. Viviana, R. Federico, R. Karin, A.J. Ya?Ez, M.D.L.A. García, R.A. Medina, C. Mónica, B. Sofía, C. Tamara, Differential subcellular distribution of glucose transporters GLUT1-6 and GLUT9 in human cancer: ultrastructural localization of GLUT1 and GLUT5 in breast tumor tissues, J. Cell. Physiol. 207 (3) (2010) 614–627, https://doi.org/10.1002/jcp.20606.

[19] M. Wuest, B.J. Trayner, T.N. Grant, H.S. Jans, J.R. Mercer, D. Murray, F.G. West, A.J.B. Mcewan, F. Wuest, C.I. Cheeseman, Radiopharmacological evaluation of 6-deoxy-6-[F]fluoro-fructose as a radiotracer for PET imaging of GLUT5 in breast cancer, Nucl. Med. Biol. 38 (4) (2011) 461–475, https://doi.org/10.1016/j.nucmedbio.2010.11.004.

[20] S. Kannan, V.V. Begoyan, J.R. Fedie, S. Xia, Ł.J. Weseliński, M. Tanasova, S. Rao, Metabolism-driven high-throughput cancer identification with GLUT5-specific molecular probes, Biosensors 8 (2) (2018) 39–50, https://doi.org/10.3390/bios8020039.

[21] Z. Jiacheng, B. Krzysztof, L. Hongxu, D. Aydan, G. Michael, M.H. Stenzel, Fructose-coated nanoparticles: a promising drug nanocarrier for triple-negative breast cancer therapy, Chem. Commun. 50 (100) (2014) 15928–15931, https://doi.org/10.1039/C4CC06651K.

[22] R.O. Hynes, Integrins: a family of cell surface receptors, Cell 48 (4) (1987) 549–554, https://doi.org/10.1016/0092-8674(87)90233-9.

[23] M.J. Humphries, Integrin structure, Biochem. Soc. Trans. 28 (4) (2000) 311–339, https://doi.org/10.1042/0300-5127:0280311.

[24] A. Duro-Castano, E. Gallon, C. Decker, M.J. Vicent, Modulating angiogenesis with integrin-targeted nanomedicines, Adv. Drug Deliv. Rev. (2017) 101–119, https://doi.org/10.1016/j.addr.2017.05.008.

[25] P. Carmeliet, Mechanisms of angiogenesis and arteriogenesis, Nat. Med. 6 (4) (2000) 389–395, https://doi.org/10.1038/74651.

[26] B. Katja, M. Claudia, B. Jürgen, Expression profiling reveals genes associated with transendothelial migration of tumor cells: a functional role for alphav-beta3 integrin, Int. J. Cancer 121 (9) (2010) 1910–1918, https://doi.org/10.1002/ijc.22879.

[27] K. Wu, C. Ru, Z. Jian, F. Meng, D. Chao, Z. Zhong, Micellar nanoformulation of lipophilized bortezomib: high drug loading, improved tolerability and targeted treatment of triple negative breast cancer, J. Mater. Chem. B 5 (28) (2017) 5658–5667, https://doi.org/10.1039/C7TB01297G.

[28] Q. Fu, Y. Zhao, Z. Yang, Q. Yue, W. Xiao, Y. Chen, Y. Yang, L. Guo, Y. Wu, Liposomes actively recognizing the glucose transporter GLUT1 and integrin alphav beta3 for dual-targeting of glioma, Arch. Pharm. 352 (2) (2019) 1800219–1800229, https://doi.org/10.1002/ardp.201800219.

[29] Y. Xue, W. He, L. Wan-Liang, D. Ju, G. Jia, T. Wei, M. Ying, Z. Yan, L. Ruo-Jing, Y. Ting-Yuan, Dual-targeting daunorubicin liposomes improve the therapeutic efficacy of brain glioma in animals, J. Control. Release Off. J. Control. Release Soc. 141 (2) (2010) 183–192, https://doi.org/10.1016/j.jconrel.2009.09.020.

[30] A. Tatibouët, J. Yang, C. Morin, G.D. Holman, Synthesis and evaluation of fructose analogues as inhibitors of the d-fructose transporter GLUT5, Bioorg. Med. Chem. 8 (7) (2000) 1825–1833, https://doi.org/10.1016/S0968-0896(00)00108-5.

[31] Y. Jing, D. James, T.T. Arnaud, H. Yasumaru, G.D. Holman, Development of high-affinity ligands and photoaffinity labels for the D-fructose transporter GLUT5, Biochem. J. 367 (2) (2002) 533–539, https://doi.org/10.1042/bj20020843.

[32] J. Levi, C.O.G. Zhen, Fluorescent fructose derivatives for imaging breast cancer cells, Bioconjug. Chem. 18 (3) (2007) 628–634, https://doi.org/10.1021/bc060184s.

[33] J.P. Xiong, T. Stehle, R. Zhang, A. Joachimiak, M. Frech, S.L. Goodman, M.A. Arnaout, Crystal structure of the extracellular segment of integrin alpha Vbeta3 in complex with an Arg-Gly-Asp ligand, Science 296 (5565) (2002) 151–155, https://doi.org/10.1126/science.1069040.

[34] B. Qu, X. Li, M. Guan, X. Li, L. Hai, Y. Wu, Design, synthesis and biological evaluation of multivalent glucosides with high affinity as ligands for brain targeting liposomes, Eur. J. Med. Chem. 72 (1) (2014) 110–118, https://doi.org/10.1016/j.ejmech.2013.10.007.

[35] Y. Peng, Y. Zhao, Y. Chen, Z. Yang, L. Zhang, W. Xiao, J. Yang, L. Guo, Y. Wu, Dual-targeting for brain-specific liposomes drug delivery system: synthesis and preliminary evaluation, Bioorg. Med. Chem. 26 (16) (2018) 4677–4686, https://doi.org/10.1016/j.bmc.2018.08.006.

[36] T. Lammers, F. Kiessling, W.E. Hennink, G. Storm, Drug targeting to tumors: principles, pitfalls and (pre-) clinical progress, J. Control. Release 161 (2) (2012) 175–187, https://doi.org/10.1080/10717544.2018.1431978.

[37] E. Wisse, F. Braet, D. Luo, R.D. Zanger, D. Jans, E. Crabbe, A.N. Vermoesen, Structure and function of sinusoidal lining cells in the liver, Toxicol. Pathol. 24 (1) (1996) 100–111, https://doi.org/10.1177/019262339602400114.

[38] K. Murugan, Y.E. Choonara, P. Kumar, D. Bijukumar, L.C.D. Toit, V. Pillay, Parameters and characteristics governing cellular internalization and trans-barrier trafficking of nanostructures, Int. J. Nanomed. 10 (2015) 2191–2206, https://doi.org/10.2147/IJN.S75615.

[39] Z. Lei, F. Yu, A.J. Cole, B. Chertok, A.E. David, J. Wang, V.C. Yang, Gum Arabic-coated magnetic nanoparticles for potential application in simultaneous magnetic targeting and tumor imaging, AAPS J. 11 (4) (2009) 693–699, https://doi.org/10.1208/s12248-009-9151-y.

[40] R. Tong, J. Cheng, Anticancer polymeric nanomedicines, Polym. Rev. 47 (3) (2007) 345–381, https://doi.org/10.1080/15583720701455079.

[41] K. Shi, J. Li, Z. Cao, P. Yang, Y. Qiu, B. Yang, Y. Wang, Y. Long, Y. Liu, Q. Zhang, A pH-responsive cell-penetrating peptide-modified liposomes with active recognizing of integrin αvβ3 for the treatment of melanoma, J. Control. Release 217 (2015) 138–150, https://doi.org/10.1016/j.jconrel.2015.09.009.

[42] K. Bauer, C. Mierke, J. Behrens, Expression profiling reveals genes associated with transendothelial migration of tumor cells: a functional role for alphav-beta3 integrin, Int. J. Cancer 121 (9) (2007) 1910–1918, https://doi.org/10.1002/ijc.22879.

[43] A. Srivatsan, M. Ethirajan, S.K. Pandey, S. Dubey, X. Zheng, T.H. Liu, M. Shibata, J. Missert, J. Morgan, R.K. Pandey, Conjugation of cRGD peptide to chlorophyll

a based photosensitizer (HPPH) alters its pharmacokinetics with enhanced tumor-imaging and photosensitizing (PDT) efficacy, Mol. Pharm. 8 (4) (2011) 1186–1197, https://doi.org/10.1021/mp200018y.
[44] H.Y. Nam, S.M. Kwon, H. Chung, S.-Y. Lee, S.-H. Kwon, H. Jeon, Y. Kim, J.H. Park, J. Kim, S. Her, Cellular uptake mechanism and intracellular fate of hydrophobically modified glycol chitosan nanoparticles, J. Control. Release 135 (3) (2009) 259–267, https://doi.org/10.1016/j.jconrel.2009.01.018.
[45] M. Tamaru, H. Akita, T. Fujiwara, K. Kajimoto, H. Harashima, Leptin-derived peptide, a targeting ligand for mouse brain-derived endothelial cells via macropinocytosis, Biochem. Biophys. Res. Commun. 394 (3) (2010) 587–592, https://doi.org/10.1016/j.bbrc.2010.03.024.
[46] X. Kai, L. Yuanpei, L. Juntao, J.S. Lee, X. Wenwu, A.M. Gonik, R.G. Agarwal, K.S. Lam, The effect of surface charge on in vivo biodistribution of PEG-oligocholic acid based micellar nanoparticles, Biomaterials 32 (13) (2011) 3435–3446, https://doi.org/10.1016/j.biomaterials.2011.01.021.
[47] P.K. Dubey, V. Mishra, S. Jain, S. Mahor, S.P. Vyas, Liposomes modified with cyclic RGD peptide for tumor targeting, J. Drug Target. 12 (5) (2004) 257–264, https://doi.org/10.1080/10611860410001728040.
[48] Z. Hu, L.Y.P. Fang, Arg-Gly-Asp (RGD) peptide conjugated poly (lactic acid)-poly(ethylene oxide) micelle for targeted drug delivery, J. Biomed. Mater. Res. A 85A (3) (2010) 797–807, https://doi.org/10.1002/jbm.a.31615.
[49] X. Xiao-Bing, H. Yue, L. Wan-Liang, Z. Xuan, Z. Hua, N. Tsuneji, Z. Qiang, Enhanced intracellular delivery and improved antitumor efficacy of doxorubicin by sterically stabilized liposomes modified with a synthetic RGD mimetic, J. Control. Release 107 (2) (2005) 262–275, https://doi.org/10.1016/j.jconrel.2005.03.030.
[50] M. NILSSON, Constituents of pollen, Acta Chem. Scand. 10 (3) (1956) 413–415.
[51] F. Han, S. Kairong, H. Guanlian, Y. Yuting, K. Qifang, L. Libao, Z. Li, C. Wenfei, D. Mingling, C. Yantao, Tumor-targeted paclitaxel delivery and enhanced penetration using TAT-decorated liposomes comprising redox-responsive poly(ethylene glycol), J. Pharm. Sci. 104 (3) (2015) 1160–1173, https://doi.org/10.1002/jps.24291.